Luminescence in undoped and Nb-doped SrTiO3 crystals: Bulk and surface emission

Shabnam Dadgostar, Jose Luis Pura Ruiz, Jorge Serrano Gutierrez, Bruno Lépine, Philippe Schieffer, Juan Jimenez

Materials Science and Engineering B 283 (2022) 115830

Contents lists available at ScienceDirect

Materials Science & Engineering B

journal homepage: www.elsevier.com/locate/mseb

Luminescence in undoped and Nb-doped $SrTiO_3$ crystals: Bulk and surface emission

Shabnam Dadgostar [a], Jose Luis Pura Ruiz [a], Jorge Serrano Gutierrez [a], Bruno Lepine [b], Philippe Schieffer [b], Juan Jimenez [a,*]

[a] GdS-Optronlab, Física de la Materia Condensada, Universidad de Valladolid, Paseo de Belén, 19, 47011 Valladolid, Spain
[b] Univ Rennes, CNRS, IPR (Institut de Physique de Rennes) –UMR 6251, F-35000 Rennes, France

ARTICLE INFO

Keywords:
Strontium titanate
Cathodoluminescence
Photoluminescence
Self-trapped holes
Small polaron

ABSTRACT

The luminescence of $SrTiO_3$ depends on the sample type, either doped or stoichiometric, as grown or treated, the excitation conditions, and temperature. The origin of the luminescence emissions, blue, green, and infrared, remains controversial. In particular, the role played by defects, mainly oxygen vacancies, impurities, and self-trapped holes and electrons on the different emissions are far to be elucidated. We present a cathodoluminescence (CL) and photoluminescence (PL) study of undoped and Nb-doped samples. The different excitation conditions of CL and PL permit to distinguish the luminescence emission from the bulk (CL) and from a surface skin region (PL). Significant differences between both techniques are seen for the undoped sample, while the Nb-doped sample presents less differences, highlighting the role played by the surface defects and the doped electrons. The study is complemented by the temperature dependence of the luminescence spectra and the emission due to defects generated by plastic deformation.

1. Introduction

Strontium Titanate (STO) presents a wide range of electrical and optical properties that make it an utterly attractive material; namely, STO is suitable for tunable dielectric devices, dynamic random-access memories, high permittivity gates, photocatalysis agent for hydrogen generation from water splitting, and substrates for other perovskite oxides [1–3].

Stoichiometric STO is a fascinating insulating ferroelectric material with a perovskite cubic crystal structure at room temperature - Pm3m space group - and an indirect energy bandgap 3.2–3.3 eV [4]. Electrical conductivity can be tuned over several orders of magnitude by combining tailored doping with annealing in reducing atmospheres. Electron doping can be achieved through oxygen vacancies and/or doping with different elements, such as Nb, Y, Sb, La. Small amounts of dopants can significantly affect the electrical state of STO, turning it from an insulator into a semiconductor, a metal, or even a superconductor [5]. The Fermi level location can be changed by varying the growth conditions, particularly by the presence of impurities and/or intrinsic defects. Mass spectrographic techniques indicate the existence of indium (In), iron (Fe), and chromium (Cr) as the most common residual impurities in undoped STO crystals [6]. Post-growth processing, e.g., annealing in reducing atmosphere, irradiation with Ar^+ ions or high energy electrons, also contribute to defect formation, which, in turn, changes the Fermi level position and thereby the STO electronic and optical properties [1,7,8].

Despite the great interest earned, there is considerable controversy about the role of defects in the STO optical properties. Photoluminescence (PL) of STO has been widely studied since the 1960 s as a unique way to access information about both the bandgap, impurities, dopants, and defect-related energy levels [1–8]. However, the interpretation of STO PL spectra is not straightforward due to the diversity of the studied specimens, namely, the growth method, doped/undoped, stoichiometry, processed/unprocessed, among others, and the different excitation conditions used. A thorough understanding of the features observed in STO luminescence obtained under varying conditions will contribute to design tailored substrates and STO-based materials for specific optoelectronic applications and enhance the capacity to tune even more STO electronic properties and its optical response.

The main luminescence features are broad bands in the green spectral range (GL), peaking at around 2.4 eV. Oxygen vacancies (V_O) [2], self-trapped electrons at Ti^{3+} ions, self-trapped holes in the vicinity of an

* Corresponding author.
E-mail address: jimenez@fmc.uva.es (J. Jimenez).

https://doi.org/10.1016/j.mseb.2022.115830
Received 7 September 2021; Accepted 17 June 2022
Available online 21 June 2022

oxygen ion (O^-) [1,9,10], and self-trapped excitons (STEs) [11] are claimed to be responsible for this emission. An additional band at about 3.2 eV, close to the bandgap energy (NBE), is also observed. It is associated with the conduction to valence band transition assisted by phonons [12]. Another band, this time in the blue spectral range (BL) (≈2.8 eV), was observed at room temperature in Ar^+ ion irradiated samples [11]. BL was also reported in oxygen-deficient material [13] or in the presence of Nb donor impurities [4]. Besides all these emissions, a structured infrared band (SIR) is observed between 1.4 and 1.6 eV in undoped stoichiometric material [6,14].

The luminescence spectra appear greatly dependent on electron doping, either by intrinsic oxygen vacancy defects or by doping with Nb. A cubic to tetragonal structural transition at about 100–110 K has been reported upon a decrease of temperature accompanied by changes in the luminescence emission [15,16].

A related relevant issue is the role of the surface on the luminescence emission. In particular, the surface states and the defects close to the surface [17] within a skin depth < 1 μm seem to play a significant role in the PL emission. Differences between the cathodoluminescence surface-related and in-depth emission were observed, suggesting that the distribution of defects in the proximity of the surface and in bulk present differences relevant to the luminescence emission [2].

These observations give a complex scenario in which the role of the in-gap states in the luminescence emission prompts to be clarified. We present herein a combined cathodoluminescence (CL) and photoluminescence study of undoped and Nb-doped $SrTiO_3$ crystals. The study is based on different excitation conditions by changing the electron beam energies for CL measurements and above and below bandgap light excitation for PL measurements. The temperature dependence of both the CL and PL spectra between 80 and 300 K was also studied. Furthermore, to ascertain the vibronic nature of SIR emission (≈1.55 eV), we combined PL with Raman experiments in undoped samples. Besides, we investigated the role of the structural transition from tetragonal to cubic phase at 100–110 K in the dependence of the luminescence emission with temperature.

2. Materials and methods

The (0 0 1)-oriented SrTiO3 single crystals were purchased from SurfaceNet (purity 99.99%). Our study was conducted on $SrTiO_3$ samples doped with Nb at 0.5 wt% ($1.7x10^{20}$ cm^{-3}), and an undoped one. Both were analyzed without prior surface treatment (as received). The undoped STO specimen was transparent, while the Nd-doped one presented a gray color.

The CL measurements were carried out with a MonoCL2 system (Gatan, UK) attached to a field emission scanning electron microscope (FESEM, Zeiss Leo 1530). The detector was a Peltier cooled CCD, and the e-beam energy was varied between 10 and 30 keV, which permits a penetration depth range from 300 nm for 10 keV to 2 μm for 30 keV as calculated by Monte-Carlo simulations [18]. The CL spectra were recorded between 80 K and 300 K.

PL and Raman measurements were carried out using a Labram UV HR 800 spectrometer (Horiba). 150 lines/mm grating was used to collect the PL spectra, while a 2400 lines/mm grating was utilized for Raman measurements. The PL measurements were carried out under excitation with three different laser lines: 325 nm from a He-Cd laser, 532 nm from a frequency-doubled Nd-YAG laser, and 633 nm from a He-Ne laser. Excitation with 325 nm laser generates electron-hole pairs, while 532 and 633 nm laser excitations will induce internal excitations at defect levels. The measurements, both Raman and PL, were performed between 80 K and 300 K.

3. Results

3.1. Cathodoluminescence

As opposed to PL, the e-beam can penetrate >2 μm deeper into the sample. Therefore, one can argue that in CL measurements with high electron energy, one probes the bulk luminescence emission, minimizing the role of the surface. Meanwhile, PL presents a more substantial influence on the surface due to the low probe depth of above bandgap light excitation (≈100 nm for 325 nm laser) [19]. Typical low temperature (80 K) CL spectra of undoped and Nb-doped samples for e-beam excitation energies with different probe depths (e-beam energies from10 to 30 keV) are shown in Fig. 1. The probe depths for these e-beam energies, calculated by Montecarlo software Casino [18], vary from ≈ 200 nm to 2 μm, Fig. 2. Therefore, at high e-beam energy, one probes the bulk CL emission, while for low e-beam energy, a region closer to the surface is examined. A skin thickness of about 1 μm with an enhanced concentration of dislocations has been reported for STO crystals [20].

The broad GL band observed at 2.25 eV is significantly more intense in the doped sample than in the undoped sample, for which it appears a factor 4 times weaker. This result agrees with that reported by Leonelli et al., who claimed a weak GL emission above 80–100 K in undoped STO [21].

The CL emission of the undoped sample presents a structured infrared band between 1.4 and 1.6 eV (SIR), which is the dominant one in this sample. The SIR band appears greatly enhanced for high e-beam energies suggesting that the SIR emission mainly arises from the bulk (depth > 1 μm). Interestingly, the SIR emission does not appear in the Nb-doped sample.

In the undoped sample, the GL emission does not increase with increasing the probe depth. Instead, the GL band intensity increases with the probe depth in the doped sample. The STO surface can contain extended surface states that, in turn, cause the formation of a dead layer under the e-beam excitation [22,23]. This layer is responsible for the overall low CL intensity observed for excitation with electron energies below 10 keV.

Fig. 3 displays the temperature dependence of the CL spectrum between 80 and 300 K. Relevant differences between undoped and Nb-doped samples are observed. The CL spectra were taken with 30 keV to reduce the contribution of the dead layer to the CL spectra. Therefore, the features observed in the 30 keV CL spectra are just attributed to the temperature dependence of the bulk emission. In the doped sample, the GL band peaks at 2.3 eV from 80 to 100 K, displaying an abrupt shift of the peak energy to 2.45 eV above 100 K, accompanied by a decrease in intensity (Fig. 3**a**). Simultaneously, a shoulder appears in the high-energy side of the GL that corresponds to the BL, at nearly 2.8 eV. The BL seems to increase in intensity at the expense of the GL for increasing temperature; however, both bands coexist up to room temperature. The NBE band, at 3.2 eV, is observed at low temperatures. Its intensity increases simultaneously to that of the BL band in agreement with the results reported by other authors [12,24–26].

Regarding the undoped sample, in Fig. 3**b**, one observes a sharp decrease of the GL intensity upon heating from 80 K to 100 K, being almost fully quenched at this temperature. Interestingly, the SIR band behaves in a different manner. First, its intensity slightly increases with increasing temperature up to 100 K. Then, above 100 K, a sharp intensity increase is observed, reaching the maximum intensity at 160 K. Above this temperature, it starts quenching, vanishing above 200 K.

The integrated intensity of the GL and BL as a function of temperature in the doped sample and that corresponding to the GL and SIR in the undoped sample are shown in Fig. 4. One observes the sharp quenching of the GL in the undoped sample compared to the Nb-doped sample Fig. 4b. For the doped sample, the GL remains visible up to room temperature. The BL appears at > 100 K, then increases in intensity up to 180 K, and above this point, it slowly decreases with increasing temperature following the tail of the GL temperature dependence. Below

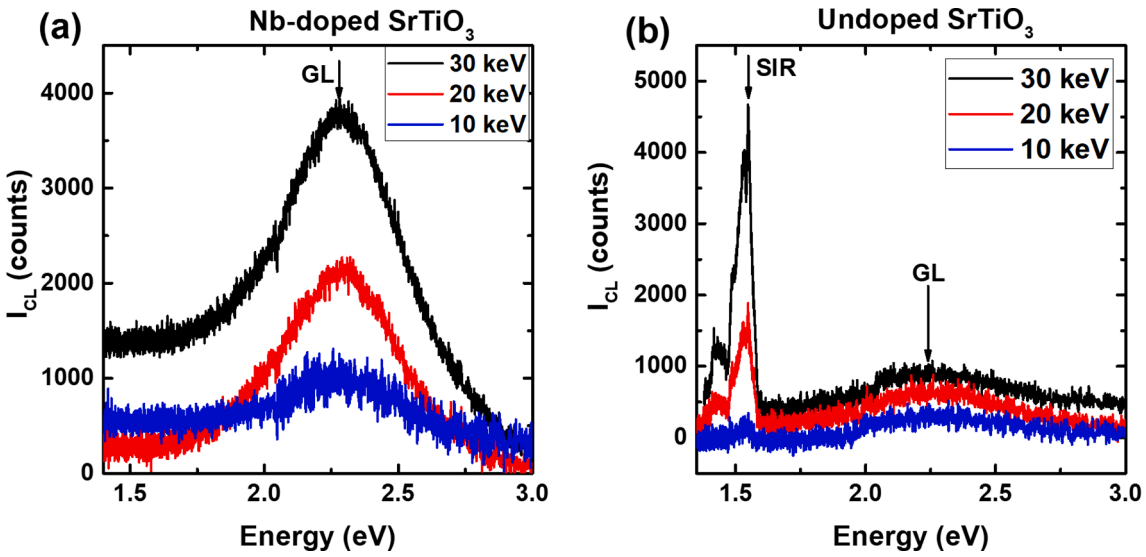

Fig. 1. CL spectra at 80 K for 10, 20 and 30 keV e-beam energies. a) Nb-doped sample, b) undoped sample.

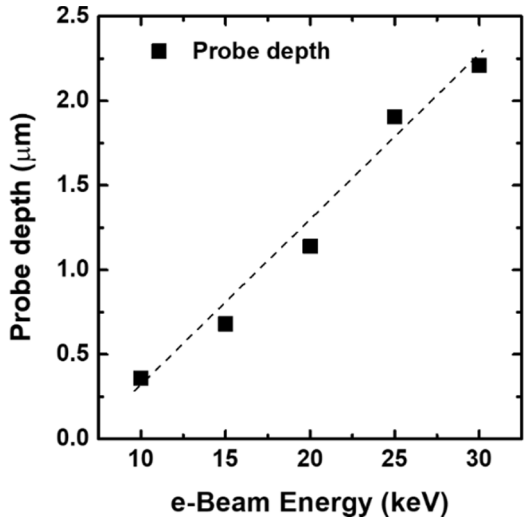

Fig. 2. Maximum electron energy loss (nominal probe depth) calculated by Montecarlo simulation using the Casino software.

160 K, the intensities of GL and BL seem to be anticorrelated, with an exchange of intensity between the two bands, while above ≈180 K, both bands follow the same temperature dependence.

As displayed in Fig. 5, the GL peak energy in the doped samples presents an abrupt shift from 2.3 to 2.45 eV at 100–110 K temperature range that roughly corresponds to the reported tetragonal-to-cubic structural phase transition, the transition temperature range is represented by the shaded area [15].

Panchromatic CL images show rather uniform CL emission for the undoped sample, while the Nb-doped sample presents inhomogeneous contrast evidencing inhomogeneous distribution of defects, Fig. 6. Local CL spectra only evidence a loss of intensity without spectral changes in the dark contrasted regions with respect to the bright contrasted areas. This rules out the existence of foreign phases with different emission signatures in our samples, contrarily to the presence of TiO_2 inclusions that were reported to be responsible for the SIR band in ref.[4].

3.2. Photoluminescence

PL spectra excited with a He-Cd laser (λ = 325 nm) at 80 K for different laser power densities (PD in the graphs) are shown in Fig. 7. The power density was varied by attenuating the laser light with optical density filters (5mW laser power at 100% transmission). One observes in both cases clean spectra with well-defined bands.

The undoped sample shows a weak but well-resolved SIR band (1.4–1.6 eV) in the low energy tail of the GL band, which peaks at 2.4 eV. GL presents high intensity with respect to what was observed in CL spectra. There is also a BL band peaking at ≈ 3.0 eV and the NBE band at 3.24 eV. All the bands appear well resolved. The intensity of the luminescence emission follows a linear dependence with the laser power density, Fig. 7**a**.

The SIR band is not observed in the doped sample under any of the used excitation conditions, in agreement with the CL results. The GL band peaks at about 2.4 eV, and the BL is not appreciable. Finally, the NBE band is well-resolved, and its intensity increases with the power density, Fig. 7**b**. The overall intensity of the luminescence emission of the doped sample is substantially higher, at least a factor 3, with respect to the undoped sample.

Fig. 8 shows selected PL spectra for temperatures ranging from 80 to 300 K, displaying a different behavior for the two samples. The GL in the undoped sample shifts smoothly from 2.41 eV at 80 K to 2.34 eV at 300 K. The intensity of the BL emission peaking at 3.0 eV first increases from 80 K to 110 K and then decreases with increasing temperature, albeit it is observable up to room temperature. Finally, the NBE band is present up to 140 K. Above this temperature, it is no longer observed. Note that BL and NBE emissions were not observed in the CL spectra of the undoped sample.

In the case of the doped sample, the GL peaks at 2.4 eV at 80 K. At 100 K, it starts monotonically shifting to higher energies reaching 2.5 eV at 140 K. Above 140 K, it remains almost unshifted with increasing temperature up to 300 K. The BL emission at 3.0 eV starts to be observed at 100 K. Its intensity increases with increasing temperature, simultaneously to the decrease of that of the GL band, in agreement with Yamada et al.[27] At 150 K, the ratio between the intensities of the GL and BL bands becomes stable, and both bands decrease simultaneously with increasing temperature, both remaining visible up to room temperature. Regarding the NBE band, its intensity increases, reaching a maximum at 110–120 K, and then starts to decrease, being barely resolved above 200 K. The thermal quenching of the GL band is sharper for the undoped sample. Furthermore, the GL band for the doped sample presents different quenching rates below and above 150 K, pointing to the thermal ionization of different in-gap states in the two temperature ranges.

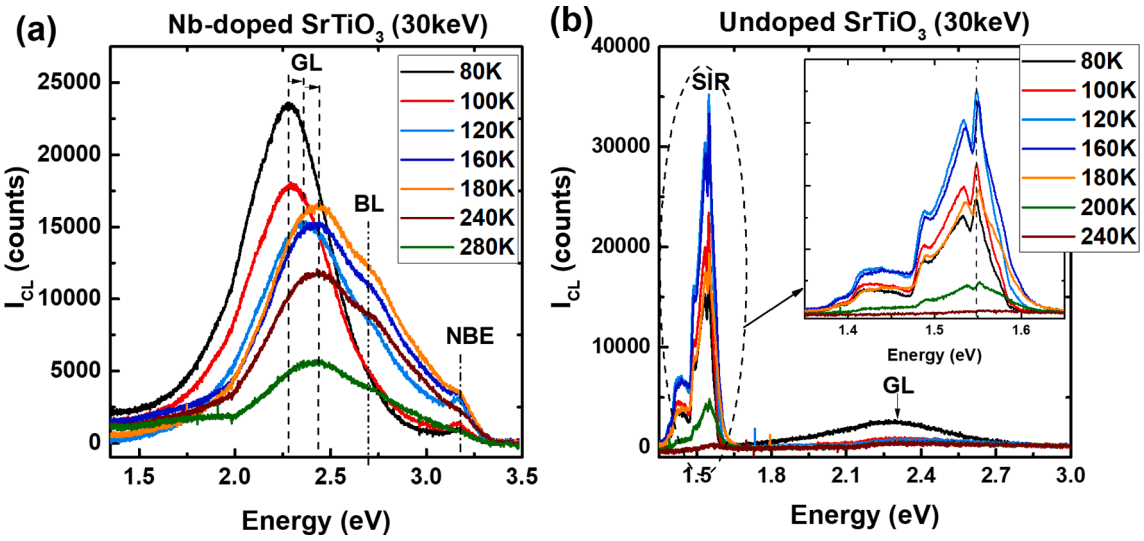

Fig. 3. CL spectra for selected temperatures between 80 and 280 K. a) Nb-doped sample, b) undoped sample (30 KeV e-beam energy).

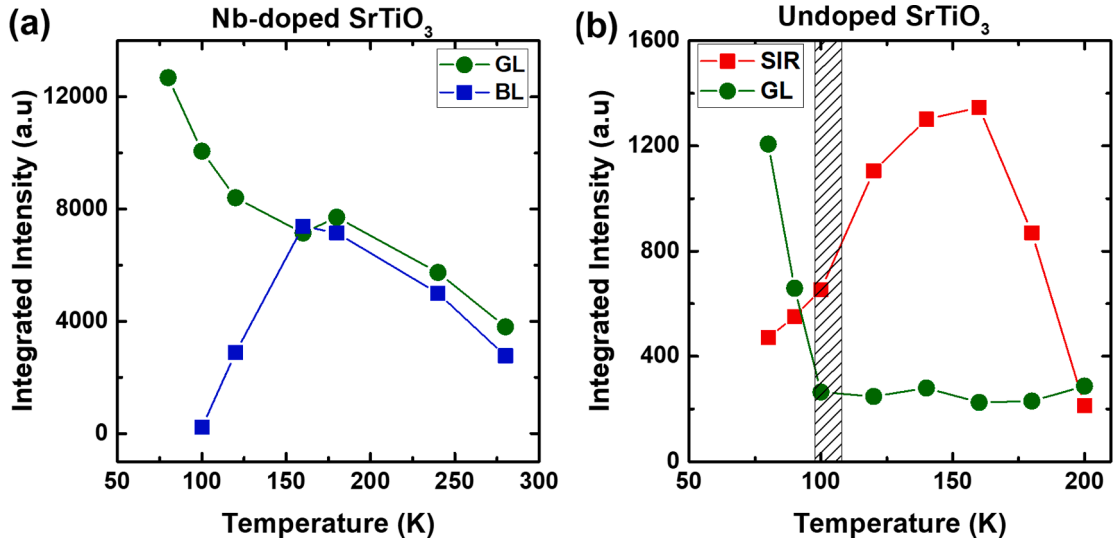

Fig. 4. a) BL and GL CL intensities vs. T (Nb-doped sample), b) GL and SIR CL intensities vs. T (undoped sample) (30 KeV e-beam energy).

The SIR band deserves special attention. It is only observed in the undoped sample. There was not even a weak contribution of this emission in the doped sample, which suggests that the presence of Nb should inhibit the centers responsible for this emission.

The SIR band presents a complex structure that can be associated with a fundamental transition and a series of vibronic replicas. It was the dominant CL emission in the undoped sample, and it was more intense for increasing the probe depth. The PL emission of the SIR band was excited with above bandgap light (325 nm), with a probe depth around 100 nm, but also can be excited with below bandgap light, either 532 nm or 633 nm, with a probe depth limited to around 1 μm because of the confocality, despite the sample transparency to these wavelengths. The three spectra are shown in Fig. 9. One observes a weak intensity for the spectrum recorded with 325 nm light excitation, although the spectrum is well-resolved. An intense emission and well-resolved spectrum for 532 nm light excitation and a weaker emission for 633 nm light excitation are observed. All three spectra display the same features, with slight differences in the background due to different activation of the luminescence emission channels. The Raman spectrum was also recorded to identify the distinct lines composing the SIR emission.

4. Discussion

There are substantial differences between CL and PL spectra. These differences can be ascribed to the region from which the luminescence signal arises in each case. The CL emission in the undoped sample was very weak for low penetration depths, and this means that the presence of surface states [28] prevents exploring the region close to the surface (<1 μm) because of the formation of a dead layer typically observed in CL [23]. Contrarily to this, the PL (excited with 325 nm light) of the undoped sample gives a well-resolved spectrum, which arises from the region close to the surface, <100 nm depth, because the low mobility of holes does not allow for the recombination volume to extend far away from the e-h generation volume [29]. One can assume that CL at high e-beam energy reveals bulk recombinations, while PL probes the top surface, which has been reported to behave differently from the volume [3,28,30]. From our results, one can argue that these differences concern both the radiative transitions involved and its temperature dependence.

Interestingly, the primary intrinsic defects in STO are the oxygen vacancies, and its formation energy at the surface is substantially lower than the bulk formation energy [30,31]. Therefore, one can expect a higher concentration of oxygen vacancies close to the surface. Indeed, it

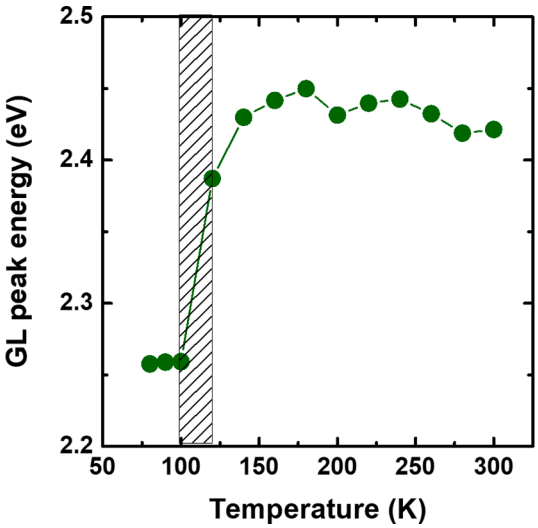

Fig. 5. GL peak energy vs. temperature (Nb-doped sample) showing the steep shift at 100–120 K (30 KeV e-beam energy), the transition temperature range is represented by the shaded area.

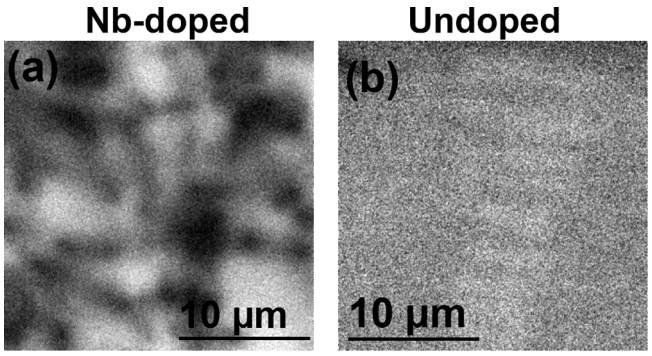

Fig. 6. Panchromatic CL (Pan-CL) images of the Nb-doped sample (a) and undoped sample (b). The undoped sample looks homogeneous, while the Nb-doped sample exhibits regions with different contrast; however, the CL spectrum does not show changes between the zones with distinct contrast, other than the intensity.

has been claimed that oxygen vacancies locate mainly near the free surface [2,30], which confers a prominent role to the oxygen deficiency in the visible emission, as it was substantially enhanced in the PL emission with respect to the CL emission in the undoped sample.

Recombination involving self-trapped-holes (STHs) is characterized by broad structureless bands, significant Stokes shift, and temperature dependence, consequences of the strong electron–phonon coupling [32]. The hole would be localized on one single O^- anion with the contribution of four neighboring oxygens; it is localized by the potential well induced by the lattice distortion around the oxygen ion [10]. The STH can recombine with free or bound electrons, or it can attract by Coulomb force an electron forming a self-trapped exciton (STE), whose recombination would emit the GL in stoichiometric STO. The emission of such transition at low temperature was calculated to be 2.51 eV, in good agreement with the experimental value reported in PL measurements. Holes are self-trapped on O^- ions with a binding energy of 13 meV, making their survival very unlikely above 100 K. Indeed, the GL band in stoichiometric samples has been reported to quench below 80 K [17,21]. In our measurements, the GL band is almost negligible in the CL spectrum of the undoped sample, which should be stoichiometric for quasi-bulk measurements performed with e-beam energy of 30 keV. Instead, it is clearly observed up to room temperature in the CL spectrum of the Nb-doped and in the PL spectra of both samples, which suggests the participation of defect states that either stabilize the STH allowing the survival of the transitions responsible for the GL or produce in-gap states accountable for the transition [33].

Small polarons form highly localized in-gap states. The small polaron formation has been shown to depend on the electron concentration, delocalizing for doping below 10^{20} cm^{-3} [33]. The luminescence emission increases with the carrier concentration, reinforcing the role of the small polarons as the main actors in the recombination process. The stability of the small polaron decreases with decreasing free electron concentration, which can account for the lower GL emission in the undoped sample. In the undoped sample, the bulk free electron concentration is low, therefore, the high e-beam energy CL measurement probing the bulk luminescence deal with a low electron doping, the electrons should be delocalized, and the GL appears very weak. On the other hand, the electron self-trapping in a perfect lattice is unstable and can only work at low temperatures [33]. Dopant impurities and intrinsic defects, including dislocations and surface reconstructions, or surface steps, favor the formation of small polarons. They are necessary to activate electron trapping [33]. This can account for the bulk GL

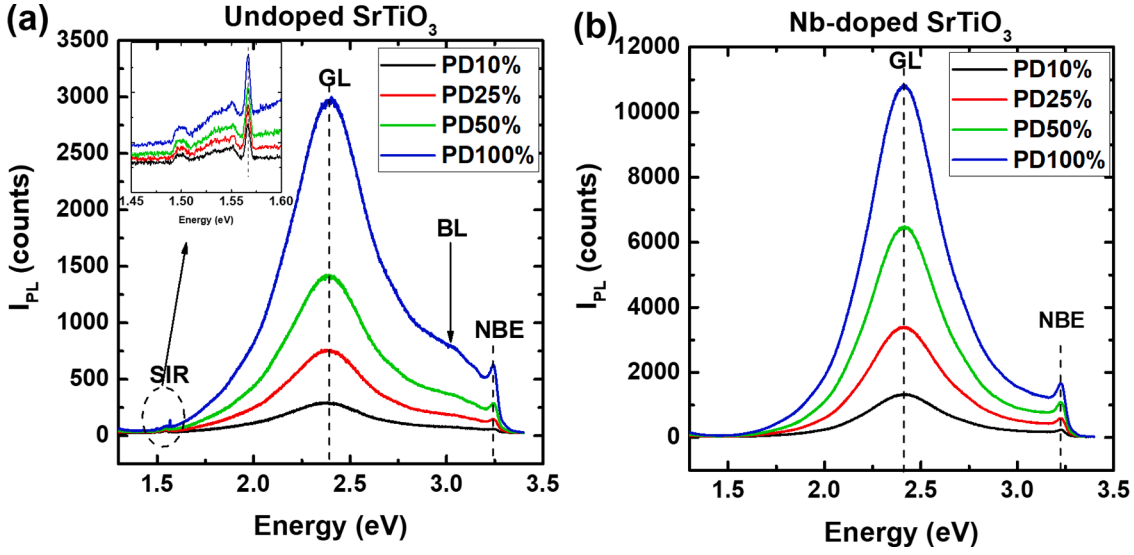

Fig. 7. PL spectra for different excitation intensities (80 K, 325 nm excitation) (a) undoped sample, (b) Nb-doped sample. The excitation intensities are selected by density filters: 100%, 50%, 25%, and 10% transmission. The inset of the panel is a magnified view of SIR spectra.

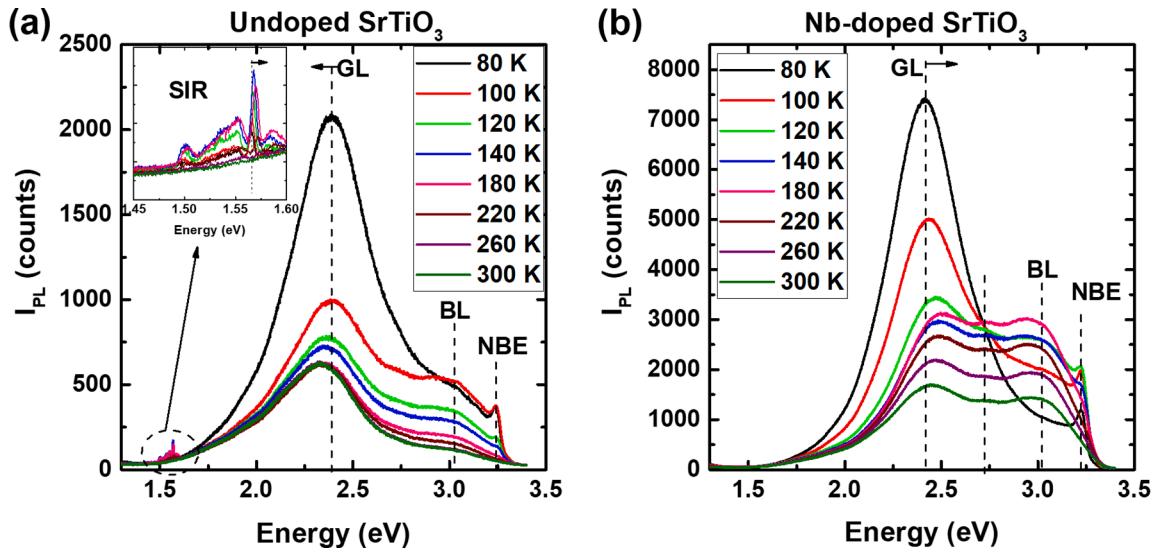

Fig. 8. PL spectra for selected temperatures between 80 and 300 K. a) undoped sample, b) Nb-doped sample. The inset of panel (a) is a magnified view of the SIR spectra.

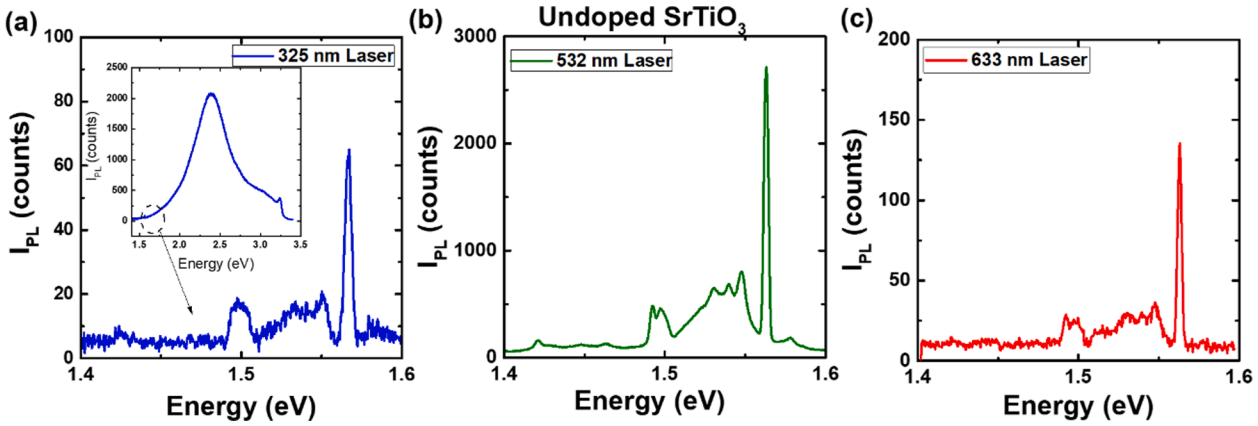

Fig. 9. SIR PL spectrum (80 K) for different excitation wavelengths. (a) 325 nm, (b) 532 nm, (c) 633 nm.

emission in the Nb-doped sample and in the surface of the undoped sample, where the defects, most likely oxygen vacancies (V_O), can activate the electron trapping. In fact, V_O and Nb should play a similar role with respect to the small polaron stability, highlighting the importance of electron doping, either Vo or Nb-doped, in the luminescence emission [33].

The intrinsic origin of the visible luminescence related to the emission of the self-trapped exciton can only account for the low-temperature emission (<100 K), as reported by R. Leonelli [21] and Kan [11]. However, the visible luminescence emission at higher temperatures, its sample dependence, and the difference in the emission between bulk and surface suggests that defects play a major role in the visible luminescence emission of STO [17]. One can argue about a low-temperature visible emission of intrinsic origin, e.g., STEs, and the visible luminescence at higher temperature related to in-gap states associated with defects, which could be the self-trapped electrons and holes that are stabilized in the vicinity of either Nb or Oxygen vacancies [33].

The evolution of emission intensity of BL and GL bands in the PL spectra of the Nb-doped sample as a function of temperature appear correlated in a similar way as observed for the CL data in Fig. 4**a**. Their temperature dependence suggests that the GL consists of a transition between two in-gap states, separated by ≈2.3 eV. At low temperature, 80 K, only the GL is observed due to the recombination from the electron trap (small polaron) to the hole trap (STH). By increasing the temperature, one of the two levels starts to be thermally unstable, and then the BL starts to be observed [27]; it should correspond to the recombination of a free carrier and the remaining in-gap state, either the electron or the hole trap. Both emissions reach similar intensity around 150 K, and subsequently, both quench with the same activation energy (30 meV), Fig. 10. This quenching would be due to the thermal disabling of the remaining in-gap state. Note that this activation energy is higher than the 13 meV binding energy reported for the STH, which means that in electron-doped, either Nb-doped or oxygen vacancies rich STO, the binding energy of the STH should be higher with respect to the stoichiometric material. This behavior suggests that GL consists of the recombination of localized electrons (small polarons or electrons trapped in a defect), while BL corresponds to the recombination of delocalized electrons. The other recombining element would be a trapped hole, common to GL and BL. It was claimed that both localized and delocalized electrons could coexist [33], which could account for the coexistence and similar behavior of GL and BL above 160 K in the doped sample. The temperature dependence of the GL in the undoped sample and the relation with the BL does not follow the same behavior as that observed for the Nb-doped sample, Fig. 8. One observes the BL at 80 K; its intensity reaches a maximum at 100 K and afterward decreases for increasing T. This different behavior suggests the existence of different defect neighborhoods giving visible emission in the same spectral

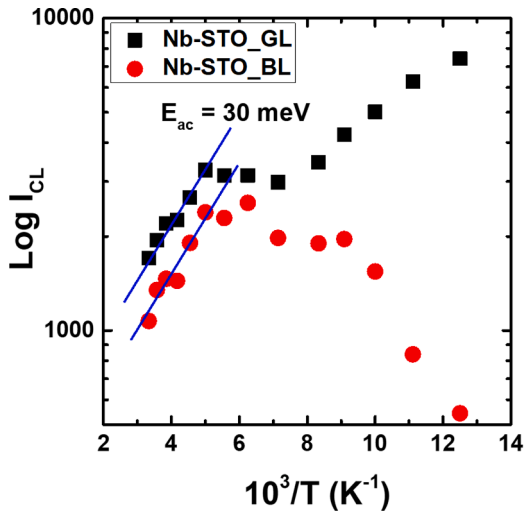

Fig. 10. BL and GL PL intensities as a function of temperature (Nb-doped sample).

window.

To get insight into the role of defects in the luminescence emission, we made scratches with a diamond tip on the two samples and measured at 80 K the CL spectra around the scratched region. The e-beam was 30 keV in order to probe the bulk emission (depth > 2 μm), reducing the influence of the surface. Selected CL spectra around the scratches are shown in Fig. 11.

The undoped sample exhibits a broad visible band formed by several overlapped Gaussian sub-bands, namely a weak GL sub-band (2.4 eV), and intense yellow (YL) (2.14 eV) and red (RL) (1.85 eV) sub-bands, which are activated by the defects created by the scratch. Note that the spectrum is uniform over the different points, but the intensity depends on the position with respect to the defect line, just being the maximum intensity at the defect line. The spectrum recorded far from scratch is also plotted as a reference. The defects created by the scratch have two consequences: a substantial enhancement of the luminescence emission, particularly the broad visible band, and a decrease of the intensity of the SIR emission, which would be the consequence of the competition with the recombination paths giving the visible emission. The presence of the yellow and red bands around the scratch can be associated with the disorder induced by the scratch [14,34]. This disorder might be related to the formation of oxygen vacancy complexes [35]. Dislocations also cause lattice distortion and provide easy paths for oxygen diffusion. An emission of around 2 eV was reported in strained and disordered STO samples [4,36], which might explain our observation in the neighborhood of the scratched region.

The luminescence emission was enhanced around the scratch for the Nb-doped sample, although less than in the undoped one. Furthermore, the GL spectral shape did not change with respect to the bare region far away from the scratched area, contrary to what was observed in the undoped sample. Furthermore, the NBE emission at 3.2 eV points up in the spectra recorded around the scratch.

The formation of oxygen vacancies by mechanical deformation has been reported by other authors [37,38]. The fact that there are no spectral changes besides the intensity variation in the Nb-doped STO contrasts with the observed changes in the undoped sample. Understanding the role of Nb in the formation of defects by mechanical deformation requires more systematic analysis, and this is out of the scope of this work. Nevertheless, one could argue about the role of Nb as an inhibitor of the formation of the defect complexes responsible for YL and RL induced by the scratch in the undoped sample. Plastic deformation around the scratch should produce vacancies and interstitials (Frenkel pairs) [39]; many of them might recombine in the Nb-doped sample, because of the position of the Fermi level, with respect to the undoped sample.

The luminescence emission is also sensitive to the cubic - tetragonal phase transition. The bulk GL is quenched at temperatures above 100–110 K in the undoped sample, Fig. 4. This temperature approximately corresponds to that of the tetragonal to the cubic structural phase transition. In the doped sample, such a quenching did not take place. Instead, the peak energy of the GL shifts steeply to higher energy between 100 and 120 K, Fig. 5, which might be related to the phase transition, suggesting a change in the lattice relaxation of either the STH or the small polaron in the cubic configuration with respect to the tetragonal one. The ionization energy deduced from the CL decay of the GL is ≈50 meV, which is slightly higher than the activation energies

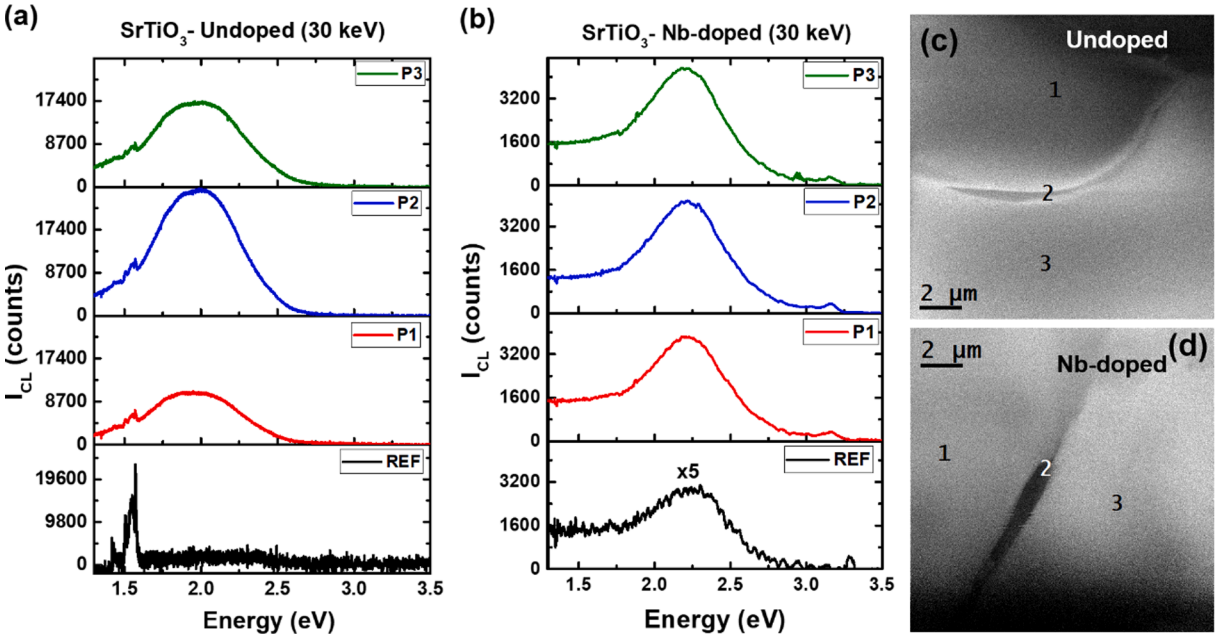

Fig. 11. CL spectra (80 K, 30KeV) in the scratched area. a) undoped sample, spectra taken at the points numbered in Pan-CL image (c), (b) Nb-doped sample, spectra taken at the points numbered in Pan-CL image (d). The spectra taken far away from the scratches are plotted as reference spectra.

reported elsewhere, 32 meV [17], 43 meV [40].

Nevertheless, the strong sample dependence of the GL emission raises some questions about its origin[16,17]. It has been argued that most of the centers giving the GL are at the specimen surface due to the presence of defects [17]. This can be true for the undoped sample, as we observe the GL mainly at the surface (PL spectra). However, it does not hold for the doped sample, for which the GL is also detected for deep probe CL. This suggests that either Nb or free electrons might enhance the bulk concentration of GL centers. The presence of Nb could support the formation of small polarons by increasing the electron concentration. A similar effect can be caused by surface defects, as seen in the PL emission of the undoped sample. The temperature dependence of the PL spectra for both undoped and doped samples does not show an abrupt change at 110 K, as observed in the CL spectra, suggesting that the transition temperature at the surface is not equivalent to that reported for the bulk. This is consistent with the change in the transition temperature caused by stress.[20] Osterman claimed a surface transition temperature of 340 K instead of 112 K of the bulk transition [41].

The SIR PL emission, exclusively observed in the undoped sample, can be decomposed in at least 10 narrow bands with the dominant one located at 1.55 eV at 80 K, frequently labeled as B-line, which was assumed to be the zero phonon line (ZPL) [14]. Most of the SIR peaks fit the Raman phonon spectrum. The intensity of the SIR bands exhibits a strong dependence on the doping species and its concentration. It was shown that Cr-doping increases its intensity with respect to undoped STO, while Sm-doping does not alter it, and Nb-doping and reducing treatments drastically quenched the SIR emission [16]. The results presented here show that it entirely disappears in the Nb-doped sample. The SIR band vanishes with the presence of Nb, as reported in ref. [4].

The ZPL has been usually associated with the B-band [14]. However, if one superimposes the Raman spectrum and the SIR spectrum, one can conclude that the ZPL corresponds to the PL peak labeled A. Shivonen also assigned the ZPL to the A peak [6]. This is easily understood if one superposes the SIR and the Raman spectra; when both are coupled, the zero frequency coincides with the PL peak A, Fig. 12 **a**. Instead, when one fixes the zero frequency at PL peak B, both PL and Raman spectra appear clearly uncoupled (Fig. 12 **b**).

Compared to the vibronic replicas, the low intensity of peak A (ZPL) accounts for an intermediate coupling with a Huang Rhys factor (S) $1 < S < 5$. In this scenario, the maximum intensity does not correspond to the ZPL, but some vibronic lines can be more intense [42].

There is a controversy about the mechanisms proposed for this emission. Crespillo et al. attributed the R-line (zero-phonon/B-line) to the $^2E_g \rightarrow {}^4A_{2g}$ transition of Cr^{3+} ion substituting a Ti^{4+}. [1] Kim et al. proposed two emission lines as the zero-phonon lines (R1 and R2) for $SrTiO_3$:Cr, which are slightly splitted (4.4×10^{-4} eV) at low temperature and broadened with increasing temperature, suggesting that it arises from magnetic dipole transitions between ^2E_g and $^4A_{2g}$ states [43]. Grabner, however, excluded Cr or Sm as the emitting centers due to the inequality of the excitation spectra of undoped STO with Cr- and Sm-doped STO. They suggested that a tightly bound center isolated from the electronic energy band, such as an intrinsic defect or a Frenkel-like exciton, can be responsible for the SIR bands [16]. Here, we postulate for internal transitions of Cr^{3+} because of the absence of emission in the Nb-doped sample. Nb and Cr occupy Ti sites in the STO lattice. One hypothesis is that Nb prevents the incorporation of Cr to Ti lattice sites.

The excitation of the SIR emission with the e-beam in CL and above bandgap light (325 nm) means that the SIR luminescence can be generated by intrinsic excitation, VB to CB. Furthermore, the SIR can also be excited by sub-bandgap light, e.g., using excitations of 532 nm and 633 nm wavelength. This suggests that it can be excited internally. Furthermore, this can allow locating the ground level ($^4A_{2g}$) in the bandgap, while the excited state (^2E_g) can be found through the SIR emission's thermal quenching.

The mechanism of SIR emission is schematically described in Fig. 13. The excitation with the above bandgap light (325 nm) produces e-h pairs. The hole is captured by Cr^{3+}, which is then transformed to Cr^{4+}. The capture of an electron in the excited state renders Cr^{4+} to excited Cr^{3+}, and the transition from the excited state to the ground state with a robust vibronic coupling gives the SIR luminescence. Excitation with sub-bandgap light (532 nm) transfers an electron from the ground state of Cr^{3+} to the conduction band ionizing Cr^{3+} to Cr^{4+}, the subsequent capture of the electron by the excited state, renders Cr^{4+} to excited Cr^{3+}, the subsequent decay into the ground state produces the SIR emission. Excitation with lower light energy (633 nm = 1.95 eV) repeats the mechanism of the 532 nm excitation but much less efficiently, suggesting that the ground state of Cr^{3+} must be approximately at 1.9 eV below the conduction band.

The SIR luminescence is thermally quenched above 160 K with an activation energy of 0.3 eV, Fig. 14. One can associate the thermal quenching with the electron thermal releasing from the excited Cr^{3+} state, switching to a non-radiative recombination path with the ground state. Note that the sum of the SIR zero-phonon line energy (peak A in Fig. 12) (1.58 eV) and the thermal activation energy (0.3 eV) is 1.88 eV,

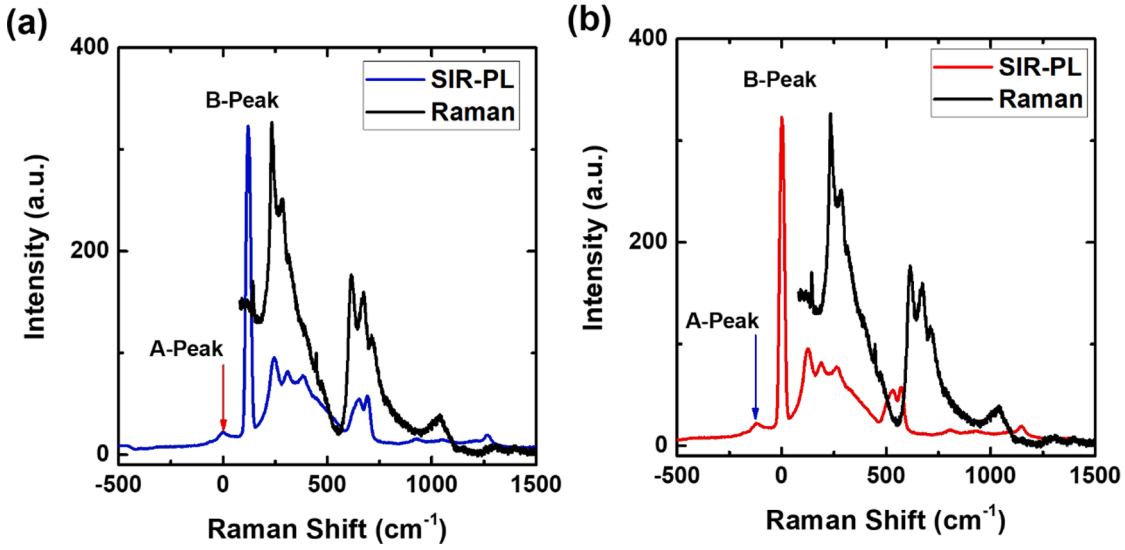

Fig. 12. PL (532 nm excitation) and Raman spectra, both at 80 K. a) The Raman spectrum and the PL vibronic spectrum are put in coincidence. The ZPL fits the peak A of the PL spectrum. b)The B line is taken as the ZPL. In this case, the vibronic PL peaks are fully decoupled from the Raman peaks.

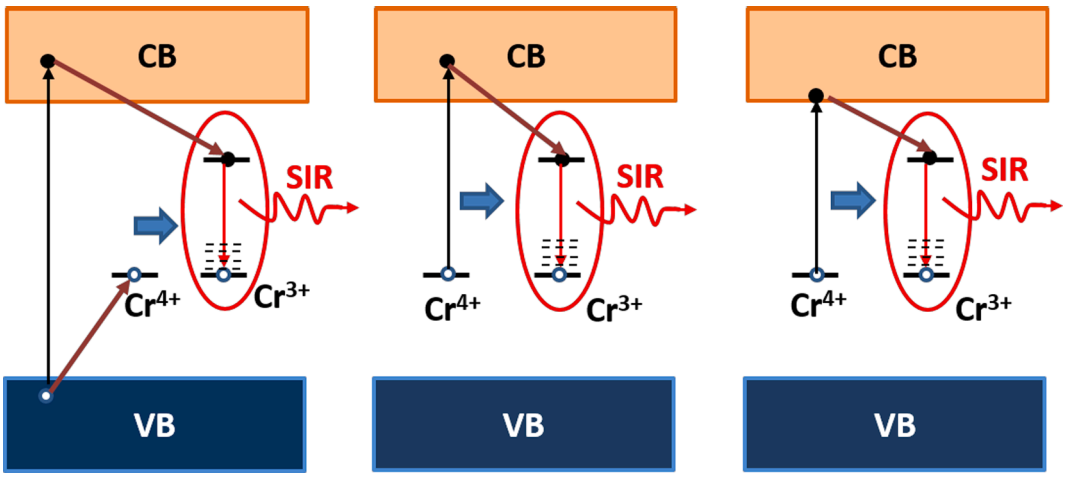

Fig. 13. Scheme of the excitation and emission mechanism of the SIR emission. a) intrinsic excitation with either the e-beam (CL) or above bandgap light (325 nm), b) excitation of Cr^{3+} with subband gap light (532 nm), c) excitation of Cr^{3+} with subband gap light (633 nm).

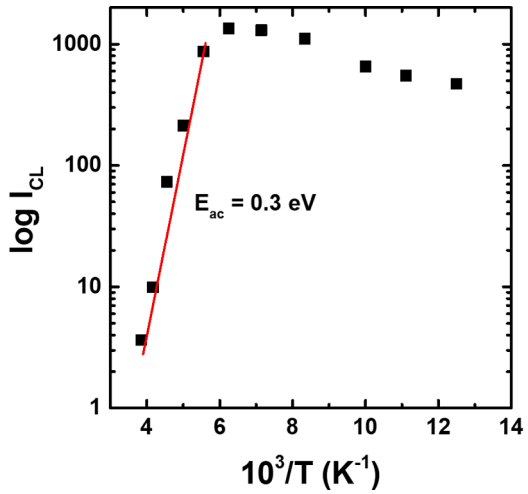

Fig. 14. SIR CL intensity vs. T.

which is very close to the 1.95 eV corresponding to the excitation with 633 nm light, which appears to be close to the threshold for exciting the SIR emission with sub-bandgap light energy.

5. Conclusions

CL and PL spectra acquired under different excitation conditions have been used to study the primary luminescence emissions of two different STO samples. The different excitation conditions have permitted to establish differences between the bulk and surface emissions. These differences are significant in the case of the undoped stoichiometric sample. The Nb-doped sample does not show such marked differences between the bulk and surface emissions, though some differences are also appreciated. This behavior gives a relevant role to Nb in the luminescence properties of the Nb-doped STO, while the undoped sample is more sensitive to the differences between the stoichiometric bulk and the defect-rich surface.

The bulk GL was quenched in the undoped sample at 100–110 K, while it was observed up to room temperature in the Nb-doped sample (both CL and PL) and in the PL of the undoped sample. This behavior was associated with the stabilization of both the STH and the small polaron by the Nb atoms in the doped sample, and lattice defects as oxygen vacancies in the surface of the undoped sample.

Temperature-dependent CL and PL measurements permitted to establish a relationship between the GL and the BL bands. This correlation differs in both samples, reinforcing the role played by Nb and lattice defects in the luminescence spectrum of STO. To confirm this, plastic deformation produced by a diamond tip was done on both samples, and the CL spectrum was measured around the scratch. The results show a significant increase of the luminescence emission in the visible range for both samples, revealing the role of defects in the luminescence emission, which is significantly enhanced with respect to the bare regions non-deformed.

A mechanism accounting for the SIR emission in the undoped sample was described by correlating the SIR emission under different excitation conditions and the Raman spectrum.

This work provides a broad scheme for STO luminescence together with the physical mechanisms giving rise to the different emissions under various circumstances concerning the type of samples, the bulk/surface analysis, the temperature, and the plastic deformation.

Declaration of Competing Interest

The authors declare that they have no known competing financial interests or personal relationships that could have appeared to influence the work reported in this paper.

Acknowledgments

This work was supported by projects VA283P18 (Junta de Castilla y Leon) and ENE2017-89561-C4-3-R (Spanish Ministry of Economics and Competitiveness), and the European Fund for Regional Development (FEDER).

References

[1] M.L. Crespillo, J.T. Graham, F. Agulló-López, Y. Zhang, W.J. Weber, Correlation between Cr3+ Luminescence and Oxygen Vacancy Disorder in Strontium Titanate under MeV Ion Irradiation, J. Phys. Chem. C. 121 (36) (2017) 19758–19766, https://doi.org/10.1021/acs.jpcc.7b04352.

[2] J. Zhang, S. Walsh, C. Brooks, D.G. Schlom, L.J. Brillson, Depth-resolved cathodoluminescence spectroscopy study of defects in SrTiO3, J. Vac. Sci. Technol. B Microelectron. Nanom. Struct. 26 (2008) 1466. https://doi.org/10.1116/1.2918315.

[3] J. Zhang, D. Doutt, T. Merz, J. Chakhalian, M. Kareev, J. Liu, L.J. Brillson, Depth-resolved subsurface defects in chemically etched SrTiO3, Appl. Phys. Lett. 94 (9) (2009) 092904, https://doi.org/10.1063/1.3093671.

[4] K.-H. Yang, T.-Y. Chen, N.-J. Ho, H.-Y. Lu, In-Gap States in Wide-Band-Gap SrTiO3 Analyzed by Cathodoluminescence, J. Am. Ceram. Soc. 94 (2011) 1811–1816, https://doi.org/10.1111/j.1551-2916.2010.04324.x.

[5] D. van der Marel, J.L.M. van Mechelen, I.I. Mazin, Common Fermi-liquid origin of T2 resistivity and superconductivity in n-type SrTiO3, Phys. Rev. B. 84 (2011), 205111, https://doi.org/10.1103/PhysRevB.84.205111.

[6] Y.T. Sihvonen, Photoluminescence, Photocurrent, and Phase-Transition Correlations in SrTiO 3, J. Appl. Phys. 38 (11) (1967) 4431–4435, https://doi.org/10.1063/1.1709142.
[7] JaeHoon Rho, S. Jung, SangWon Shin, JiHwan Kwon, M. Kim, JongHan Song, E. Choi, Blue and infrared cathodoluminescence induced by carbon-irradiation in SrTiO3 single crystal, J. Lumin. 130 (10) (2010) 1687–1689, https://doi.org/10.1016/j.jlumin.2010.03.032.
[8] S. Mochizuki, F. Fujishiro, K. Shibata, A. Ogi, T. Konya, K. Inaba, Optical, electrical, and X-ray-structural studies on Verneuil-grown SrTiO3 single crystal: Annealing study, Phys. B Condens. Matter. 401–402 (2007) 433–436, https://doi.org/10.1016/j.physb.2007.08.205.
[9] M.L. Crespillo, J.T. Graham, F. Agulló-López, Y. Zhang, W.J. Weber, Role of oxygen vacancies on light emission mechanisms in SrTiO3 induced by high-energy particles, J. Phys. D. Appl. Phys. 50 (15) (2017) 155303, https://doi.org/10.1088/1361-6463/aa627f.
[10] H. Chen, N. Umezawa, Hole localization, migration, and the formation of peroxide anion in perovskite SrTiO3, Phys. Rev. B. 90 (2014), 035202, https://doi.org/10.1103/PhysRevB.90.035202.
[11] D. Kan, T. Terashima, R. Kanda, A. Masuno, K. Tanaka, S. Chu, H. Kan, A. Ishizumi, Y. Kanemitsu, Y. Shimakawa, M. Takano, Blue-light emission at room temperature from Ar+-irradiated SrTiO3, Nat. Mater. 4 (11) (2005) 816–819, https://doi.org/10.1038/nmat1498.
[12] Y. Yamada, Y. Kanemitsu, Band-to-band photoluminescence in SrTiO3, Phys. Rev. B. 82 (2010), 121103, https://doi.org/10.1103/PhysRevB.82.121103.
[13] D. Kan, R. Kanda, Y. Kanemitsu, Y. Shimakawa, M. Takano, T. Terashima, A. Ishizumi, Blue luminescence from electron-doped SrTiO3, Appl. Phys. Lett. 88 (19) (2006) 191916, https://doi.org/10.1063/1.2202750.
[14] M. Crespillo, J. Graham, F. Agulló-López, Y. Zhang, W. Weber, Recent Advances on Carrier and Exciton Self-Trapping in Strontium Titanate: Understanding the Luminescence Emissions, Crystals. 9 (2019) 95, https://doi.org/10.3390/cryst9020095.
[15] F.W. Lytle, X-Ray Diffractometry of Low-Temperature Phase Transformations in Strontium Titanate, J. Appl. Phys. 35 (7) (1964) 2212–2215, https://doi.org/10.1063/1.1702820.
[16] L. Grabner, Localizing nature of photo-excited states in SrTiO3, Phys. Rev. 177 (1969) 1315–1323, https://doi.org/10.1103/PhysRev.177.1315.
[17] S. Mochizuki, F. Fujishiro, S. Minami, Photoluminescence and reversible photo-induced spectral change of SrTiO3, J. Phys. Condens. Matter. 17 (6) (2005) 923–948, https://doi.org/10.1088/0953-8984/17/6/011.
[18] D. Drouin, A.R. Couture, D. Joly, X. Tastet, V. Aimez, R. Gauvin, CASINO V2.42 - A fast and easy-to-use modeling tool for scanning electron microscopy and microanalysis users, Scanning. 29 (3) (2007) 92–101, https://doi.org/10.1002/sca.20000.
[19] S. Zollner, A.A. Demkov, R. Liu, P.L. Fejes, R.B. Gregory, P. Alluri, J.A. Curless, Z. Yu, J. Ramdani, R. Droopad, T.E. Tiwald, J.N. Hilfiker, J.A. Woollam, Optical properties of bulk and thin-film SrTiO3 on Si and Pt, J. Vac. Sci. Technol. B Microelectron. Nanom. Struct. 18 (2000) 2242, https://doi.org/10.1116/1.1303741.
[20] R. Wang, Y. Zhu, S.M. Shapiro, Structural Defects and the Origin of the Second Length Scale in SrTiO3, Phys. Rev. Lett. 80 (1998) 2370–2373, https://doi.org/10.1103/PhysRevLett.80.2370.
[21] R. Leonelli, J.L. Brebner, Time-resolved spectroscopy of the visible emission band in strontium titanate, Phys. Rev. B. 33 (12) (1986) 8649–8656, https://doi.org/10.1103/PhysRevB.33.8649.
[22] D.B. Wittry, D.F. Kyser, Cathodoluminescence at p - n Junctions in GaAs, J. Appl. Phys. 36 (4) (1965) 1387–1389, https://doi.org/10.1063/1.1714315.
[23] J. Jimenez, J.W. Tomm, Spectroscopic Analysis of Optoelectronic Semiconductors, 2016. http://link.springer.com/10.1007/978-3-319-42349-4.
[24] H.Y. Hwang, Oxygen vacancies shine blue, Nat. Mater. 4 (11) (2005) 803–804, https://doi.org/10.1038/nmat1515.
[25] Y. Yamada, Y. Kanemitsu, Blue light emission from strongly photoexcited and electron-doped SrTiO3, J. Appl. Phys. 109 (10) (2011) 102410, https://doi.org/10.1063/1.3577613.
[26] W. Xu, J. Yang, W. Bai, K. Tang, Y. Zhang, X. Tang, Oxygen vacancy induced photoluminescence and ferromagnetism in SrTiO3 thin films by molecular beam epitaxy, J. Appl. Phys. 114 (15) (2013) 154106, https://doi.org/10.1063/1.4825257.
[27] Y. Yamada, H. Yasuda, T. Tayagaki, Y. Kanemitsu, Temperature Dependence of Photoluminescence Spectra of Nondoped and Electron-Doped SrTiO3: Crossover from Auger Recombination to Single-Carrier Trapping, Phys. Rev. Lett. 102 (2009), 247401, https://doi.org/10.1103/PhysRevLett.102.247401.
[28] J. Hanzig, B. Abendroth, F. Hanzig, H. Stöcker, R. Strohmeyer, D.C. Meyer, S. Lindner, M. Grobosch, M. Knupfer, C. Himcinschi, U. Mühle, F. Munnik, Single crystal strontium titanate surface and bulk modifications due to vacuum annealing, J. Appl. Phys. 110 (6) (2011) 064107, https://doi.org/10.1063/1.3638692.
[29] M. Fleischer, H. Meixner, C. Tragut, Hole Mobility in Acceptor-Doped, Monocrystalline SrTiO3, J. Am. Ceram. Soc. 75 (6) (1992) 1666–1668, https://doi.org/10.1111/j.1151-2916.1992.tb04242.x.
[30] A.R. Silva, G.M. Dalpian, Oxygen vacancies at the surface of SrTiO 3 thin films, J. Appl. Phys. 115 (3) (2014) 033710, https://doi.org/10.1063/1.4861730.
[31] J. Shen, H. Lee, R. Valentí, H.O. Jeschke, Ab initio study of the two-dimensional metallic state at the surface of SrTiO3: Importance of oxygen vacancies, Phys. Rev. B. 86 (2012), 195119, https://doi.org/10.1103/PhysRevB.86.195119.
[32] J.B. Varley, A. Janotti, C. Franchini, C.G. Van de Walle, Role of self-trapping in luminescence and p-type conductivity of wide-band-gap oxides, Phys. Rev. B. 85 (2012), 081109, https://doi.org/10.1103/PhysRevB.85.081109.
[33] X. Hao, Z. Wang, M. Schmid, U. Diebold, C. Franchini, Coexistence of trapped and free excess electrons in SrTiO3, Phys. Rev. B. 91 (2015), 085204, https://doi.org/10.1103/PhysRevB.91.085204.
[34] L.E.B. Soledade, E. Longo, E.R. Leite, F.M. Pontes, F. Lanciotti Jr., C.E.M. Campos, P.S. Pizani, J.A. Varela, Room-temperature photoluminescence in amorphous SrTiO3 - the influence of acceptor-type dopants, Appl. Phys. A Mater. Sci. Process. 75 (2002) 629–632, https://doi.org/10.1007/s003390101140.
[35] D.A. Crandles, B. Nicholas, C. Dreher, C.C. Homes, A.W. McConnell, B.P. Clayman, W.H. Gong, J.E. Greedan, Optical properties of highly reduced SrTiO3-x, Phys. Rev. B. 59 (1999) 12842–12846, https://doi.org/10.1103/PhysRevB.59.12842.
[36] N.A. Kulagin, E. Hieckmann, Spectra and color centers of strontium titanate crystals, Opt. Spectrosc. 112 (1) (2012) 79–86, https://doi.org/10.1134/S0030400X12010134.
[37] Y. Wang, X. Shi, X. Lai, Z. Gao, L. Liu, Y. Wang, W. Zhu, C. Meng, L. Zhang, Fabricating Ohmic contact on Nb-doped SrTiO3 surface in nanoscale, Appl. Phys. Lett. 108 (19) (2016) 192102, https://doi.org/10.1063/1.4949475.
[38] C. Rodenbücher, S. Menzel, D. Wrana, T. Gensch, C. Korte, F. Krok, K. Szot, Current channeling along extended defects during electroreduction of SrTiO3, Sci. Rep. 9 (2019) 2502, https://doi.org/10.1038/s41598-019-39372-2.
[39] R.W. Cahn, P. Haasen, eds., Physical metallurgy, Fourth, ELSEVIER SCIENCE B.V, 1996. https://doi.org/0 444 89875 1.
[40] T. Hasegawa, M. Shirai, K. Tanaka, Localizing nature of photo-excited states in SrTiO3, J. Lumin. 87–89 (2000) 1217–1219, https://doi.org/10.1016/S0022-2313(99)00520-7.
[41] D.P. Osterman, K. Mohanty, J.D. Axe, Observation of the antiferroelectric order parameter in surface layers of SrTiO 3, J. Phys. C Solid State Phys. 21 (14) (1988) 2635–2640, https://doi.org/10.1088/0022-3719/21/14/005.
[42] G. Blasse, Vibronic transitions in rare earth spectroscopy, Int. Rev. Phys. Chem. 11 (1) (1992) 71–100, https://doi.org/10.1080/01442359209353266.
[43] Q. Kim, R.C. Powell, M. Mostoller, T.M. Wilson, Analysis of the vibronic spectrum of chromium doped strontium titanate, Phys. Rev. B. 12 (12) (1975) 5627–5642, https://doi.org/10.1103/PhysRevB.12.5627.